

Article

Modeling of Heat Distribution in Porous Aluminum Using Fractional Differential Equation

Rafał Brociek ^{1,*}, Damian Słota ¹, Mariusz Król ², Grzegorz Matula ² and Waldemar Kwaśny ²

¹ Institute of Mathematics, Silesian University of Technology, Kaszubska 23, 44-100 Gliwice, Poland; damian.slota@polsl.pl

² Institute of Engineering Materials and Biomaterials, Silesian University of Technology, Konarskiego 18A, 44-100 Gliwice, Poland; mariusz.krol@polsl.pl (M.K.); grzegorz.matula@polsl.pl (G.M.); waldemar.kwasny@polsl.pl (W.K.)

* Correspondence: rafal.brociek@polsl.pl

Received: 20 November 2017; Accepted: 9 December 2017; Published: 12 December 2017

Abstract: The authors present a model of heat conduction using the Caputo fractional derivative with respect to time. The presented model was used to reconstruct the thermal conductivity coefficient, heat transfer coefficient, initial condition and order of fractional derivative in the fractional heat conduction inverse problem. Additional information for the inverse problem was the temperature measurements obtained from porous aluminum. In this paper, the authors used a finite difference method to solve direct problems and the Real Ant Colony Optimization algorithm to find a minimum of certain functional (solve the inverse problem). Finally, the authors present the temperature values computed from the model and compare them with the measured data from real objects.

Keywords: fractional derivative; inverse problem; heat conduction in porous media; thermal conductivity; heat transfer coefficient

1. Introduction

Fractional calculus is a part of mathematical analysis and has a lot of applications in technical science. One of the most popular books about fractional calculus is Reference [1]. References [2–4] provide information about fractional calculus, fractional differential equations, approximations of fractional derivatives and numerical methods. There are also a lot of articles about fractional calculus—for example, [5–7].

Various phenomena in nature can be modeled using fractional derivatives [8–16]—for example, in [9,11], the authors surveyed fractional-order electric circuit models, Reference [12] shows applications of fractional derivatives in control theory, and, in [13,14,16,17], we can find information about application fractional derivatives in heat conduction problems. In [16], the authors present an algorithm to solve the fractional heat conduction equation. In the presented model, the heat transfer coefficient is reconstructed based on measurements of the temperature. The direct problem is solved by using the implicit finite difference method. To minimize the functional defining the error of the approximate solution, the Nelder–Mead algorithm is used. In [18], the authors consider the inverse problem of recovering a time-dependent factor of an unknown source on some sub-boundary for a diffusion equation with time fractional derivative. The authors present two regularizing schemes in order to reconstruct an unknown boundary source. Another paper where authors solved the inverse problem with fractional derivatives is Reference [19]. Zhuang et al. considered a time-fractional heat conduction inverse problem with a Caputo derivative in a three-layer composite medium. To solve the direct problem, they used a finite difference method, and, for the inverse problem, the Levenberg–Marquardt method was applied. The results show that the time-fractional heat conduction model provides an effective and accurate simulation of the experimental data. In addition,

in [20], it is considered an inverse fractional heat conduction problem. The authors show that the model with fractional derivatives better describes the process of heat conduction in ceramics media.

In this paper, the authors consider the heat conduction inverse problem. A mathematical model describing the heat transfer phenomenon in porous aluminum is given by fractional differential equation with initial-boundary conditions. In this case, we used the Caputo fractional derivative. The algorithm consists of two parts: solution of direct problem and solution of inverse problem by finding the minimum of the functional. Additional information for the inverse problem was the temperature measurements obtained from porous aluminum. The direct problem was solved using a finite difference method and approximations of Caputo derivatives [17,21]. In the inverse problem, the heat transfer coefficient, thermal conductivity coefficient, initial condition and order of derivative were sought. In order to do that, we need to minimize the functional describing the error of approximate solution. The functional was minimized by a Real Ant Colony Optimization algorithm [22,23].

More about heat conduction inverse problems can be found in [24–28]. Zielonka et al. in [25] solved the one-phase inverse problem of alloy solidifying within the casting mould. The authors also include their paper shrinkage of the metal phenomenon.

The investigated inverse problem consists of reconstruction of the heat transfer coefficient on the boundary of the casting mould on the basis of measurements of temperature read from the sensor placed in the middle of the mould. In [28], Stefan problems relevant to burning oil-water systems are considered. The author used the heat balance integral method.

2. Fractional Heat Conduction Equation

In this section, we would like to present the fractional differential equation

$$c\rho \frac{\partial^\alpha u(x,t)}{\partial t^\alpha} = \lambda \frac{\partial^2 u(x,t)}{\partial x^2}, \quad (1)$$

defined in region $D = \{(x,t) : x \in [0, L], t \in [0, T], L, T \in \mathbb{R}_+\}$, where c is specific heat, ρ is density of material, λ is thermal conductivity coefficient, α is order of derivative and u is the function describing the distribution of temperature. In literature, this equation is called the Time Fractional Diffusion Equation (TFDE). For a more precise description of the model, we still need initial-boundary conditions. In this case, we used a Neumann boundary condition for $x = 0$, and a Robin boundary condition for $x = L$. Below, we present initial-boundary conditions:

$$u(x,0) = f(x), \quad x \in [0, L], \quad (2)$$

$$-\lambda \frac{\partial u}{\partial x}(0,t) = q(t), \quad t \in [0, T], \quad (3)$$

$$-\lambda \frac{\partial u}{\partial x}(L,t) = h(t)(u(L,t) - u^\infty), \quad t \in [0, T], \quad (4)$$

where f is function describing initial condition, q is the heat flux, h is heat transfer coefficient and u^∞ is ambient temperature. By solving models (1)–(4), we obtain the temperature values at the points of the domain D . To model process of heat conduction in porous media, we used Caputo fractional derivative of order $\alpha \in (0, 1)$, which, in our case, is defined by the formula [1]:

$$\frac{\partial^\alpha u(x,t)}{\partial t^\alpha} = \frac{1}{\Gamma(1-\alpha)} \int_0^t \frac{\partial u(x,s)}{\partial s} (t-s)^{-\alpha} ds. \quad (5)$$

In the next part of the article, we use the considered model to solve the fractional heat conduction inverse problem.

3. Formulation of the Problem

In an inverse problem, some information in the considered model is unknown; in our case, we do not know: thermal conductivity coefficient λ , heat transfer coefficient h , initial condition f and order of derivative α . We have additional information, called input data, which is the temperature measurements. We denote it by:

$$u(x_p, t_j) = \hat{U}_j, \quad j = 1, 2, \dots, N_1, \quad (6)$$

where N_1 is number of measurements from thermocouples.

If we solve the direct problems (1)–(4) for fixed values of the sought parameters, then we obtain calculated values of the temperature at certain fixed points of the domain D —in our case, we denote it by $U_j(\lambda, h, f, \alpha)$. Using the calculated values of the temperature $U_j(\lambda, h, f, \alpha)$, input data \hat{U}_j , we create functionals defining the error of approximate solution:

$$F(\lambda, h, f, \alpha) = \sum_{j=1}^{N_1} (U_j(\lambda, h, f, \alpha) - \hat{U}_j)^2. \quad (7)$$

By minimizing the functional (7), we find the approximate values of the sought parameters.

The measured temperatures (input data) \hat{U}_j were obtained from a sample of porous aluminum. This sample was formed by pressurizing the powders' aluminum of medium size 0.8 mm in the plate hydraulic press. Powders were pressed at 150 bar pressure. Sample was heated to 300 °C at speed of 1 K/s and then cooled to ambient temperature. During that time, sample temperature measurements were done, which measurements were used as input data for algorithm.

4. Method of Solution

The solution of the inverse problem can be divided into two parts: first—solution of direct problems (1)–(4), and second—finding minimum of the functional (7).

4.1. Solution of the Direct Problem

In solving the inverse problem, we have to solve the direct problem many times. To solve direct problems (1)–(4), we used implicit finite difference scheme. In order to do that, we create grid

$$S = \{(x_i, t_k), x_i = i \Delta x, t_k = k \Delta t, i = 0, 1, \dots, N, k = 0, 1, 2, \dots, M\},$$

with size $(N + 1) \times (M + 1)$ and steps $\Delta x = L/N$, $\Delta t = T/M$. Caputo fractional derivative (5) is approximated by the formula [17]:

$$\frac{\partial^\alpha u}{\partial t^\alpha}(x_i, t_k) \approx D_t^\alpha u_i^k = \sigma(\alpha, \Delta t) \sum_{j=1}^k \omega(\alpha, j) (u_i^{k-j+1} - u_i^{k-j}), \quad (8)$$

where

$$\sigma(\alpha, \Delta t) = \frac{1}{\Gamma(1 - \alpha) (1 - \alpha) (\Delta t)^\alpha},$$

$$\omega(\alpha, j) = j^{1-\alpha} - (j - 1)^{1-\alpha}.$$

We also need to approximate boundary conditions of the second and third kinds. The following approximations were used:

$$-\lambda_0 \frac{u_1^k - u_{-1}^k}{2\Delta x} = q_k \implies u_{-1}^k = u_1^k + \frac{2\Delta x q_k}{\lambda_0}, \quad (9)$$

$$-\lambda_N \frac{u_{N+1}^k - u_{N-1}^k}{2\Delta x} = h_k(U_N^k - u^\infty) \implies u_{N+1}^k = u_{N-1}^k - \frac{2\Delta x h_k}{\lambda_N} (u_N^k - u^\infty). \tag{10}$$

Using all approximations (8)–(10) and the differential quotient for the derivative of second order with respect to space

$$\frac{\partial^2 u}{\partial x^2} (x_i, t_k) \approx \frac{u_{i-1}^k - 2u_i^k + u_{i+1}^k}{(\Delta x)^2},$$

we get the following differential equations

$k \geq 1, i = 0:$

$$\left(\sigma(\alpha, \Delta t) + \frac{2a_0}{(\Delta x)^2}\right) u_0^k - \frac{2a_0}{(\Delta x)^2} u_1^k = \sigma(\alpha, \Delta t) u_0^{k-1} - \sigma(\alpha, \Delta t) \sum_{j=2}^k \omega(\alpha, j) (u_0^{k-j+1} - u_0^{k-j}) + \frac{2q_k}{c \rho \Delta x},$$

$k \geq 1, i = 1, 2, \dots, N - 1:$

$$\begin{aligned} -\frac{a_i}{(\Delta x)^2} u_{i-1}^k + \left(\sigma(\alpha, \Delta t) + \frac{2a_i}{(\Delta x)^2}\right) u_i^k - \frac{a_i}{(\Delta x)^2} u_{i+1}^k \\ = \sigma(\alpha, \Delta t) u_i^{k-1} - \sigma(\alpha, \Delta t) \sum_{j=2}^k \omega(\alpha, j) (u_i^{k-j+1} - u_i^{k-j}), \end{aligned}$$

$k \geq 1, i = N:$

$$\begin{aligned} -\frac{2a_N}{(\Delta x)^2} u_{N-1}^k + \left(\sigma(\alpha, \Delta t) + \frac{2a_N}{(\Delta x)^2} + \frac{2}{c \rho \Delta x} h_k\right) u_N^k \\ = \sigma(\alpha, \Delta t) u_N^{k-1} - \sigma(\alpha, \Delta t) \sum_{j=2}^k \omega(\alpha, j) (u_N^{k-j+1} - u_N^{k-j}) + \frac{2}{c \rho \Delta x} h_k u^\infty, \end{aligned}$$

where $u_i^k \approx u(x_i, t_k)$, $h_k = h(t_k)$, $q_k = q(t_k)$ and $a_i = \frac{\lambda(x_i)}{c \rho}$ is the thermal diffusivity coefficient. Solving the system of equations gives us approximate values of function u in points of grid S . More about stability of the presented method can be found in [17].

4.2. Minimum of the Functional

The second part of the presented algorithms is finding the minimum of the functional (7). In this paper, we used the Real Ant Colony Optimization algorithm (Algorithm 1). The algorithm was inspired by the behavior of swarm of ants in nature. Pheromone spots, which are L , are identified with solutions. Firstly, they are distributed randomly in the considered area. Then, we rank them according to their quality—better solution means stronger pheromone spot and greater probability to choose it by ant. In this way, we create the solution archive. In every iteration, the one of M ants constructs one new solution (new pheromone spot) using the probability density function (in this case, Gaussian function). The ant chooses with the probability a pheromone spot (solution) and transforms it by sampling its neighborhood using the Gaussian function. Then, the solutions archive is updated with new solutions and sorted according to the quality; next, M worst solutions are rejected. The described algorithm was adapted for parallel computing. For the description of the algorithm, we will introduce the symbols:

$F(\mathbf{x})$	minimized function, $\mathbf{x} = (x_1, \dots, x_n) \in D$
n	dimension (number of variables)
nT	number of threads
$M = nT \cdot p$	number of ants in population
I	number of iterations
L	number of pheromone spots
q, ζ	parameters of the algorithm

Algorithm 1: Parallel Real ACO algorithm**Initialization of the algorithm**

1. Setting input parameters of the algorithm L, M, I, nT, q, ξ .
2. Randomly generate L pheromone spots (solutions) and assign them to set T_0 (starting archive).
3. Calculate values of the minimized function F for each pheromone spot and sort the archive T_0 from best to worst solution.

Iterative process

4. Assigning probabilities to pheromone spots (solutions) according to the following formula:

$$p_l = \frac{\omega_l}{\sum_{l=1}^L \omega_l} \quad l = 1, 2, \dots, \quad (11)$$

where weights ω_l are associated with l -th solution and expressed by the formula

$$\omega_l = \frac{1}{qL\sqrt{2\pi}} \cdot e^{-\frac{(l-1)^2}{2q^2L^2}}.$$

5. Ant chooses a random l -th solution with probability p_l .
6. Ant transforms the j -th coordinate ($j = 1, 2, \dots, n$) of l -th solution s_j^l by sampling proximity with the probability density function (Gaussian function)

$$g(x, \mu, \sigma) = \frac{1}{\sigma\sqrt{2\pi}} \cdot e^{-\frac{(x-\mu)^2}{2\sigma^2}},$$

where $\mu = s_j^l$, $\sigma = \frac{\xi}{L-1} \sum_{p=1}^L |s_j^p - s_j^l|$.

7. Repeat steps 5–6 for each ant. We obtain M new solutions (pheromone spots).
8. Divide new solutions on nT groups. Calculate values of minimized function F for each new solution (parallel computing).
9. Add to the archive T_i new solutions, sort the archive by quality of solutions, remove M worst solution.
10. Repeat steps 4–9 I times.

5. Results

In this section, we present the obtained results. We consider models (1)–(4) with the following data:

$$t \in [0, 71.82][\text{s}], \quad x \in [0, 3.825][\text{mm}], \quad c = 900 \left[\frac{\text{J}}{\text{kg} \cdot \text{K}} \right], \quad q = 2106 \left[\frac{\text{kg}}{\text{m}^3} \right],$$

$$q(t) = 0 \left[\frac{\text{W}}{\text{m}^2} \right], \quad u^\infty = 298 [\text{K}], \quad x_p = 3.825 [\text{mm}].$$

In the presented model, we lack the following data:

- $\lambda = a_1 \left[\frac{\text{J}}{\text{s}^\alpha \cdot \text{m} \cdot \text{K}} \right]$ —modified thermal conductivity coefficient,
- $f(x) = a_2 [\text{K}]$ —initial condition,
- $h(t) = a_3 t^2 + a_4 t + a_5 \left[\frac{\text{W}}{\text{m}^2 \cdot \text{K}} \right]$ —heat transfer coefficient,
- $\alpha = a_6$ —order of derivative,

which is reconstructed based on measurements of temperature. We assume that

$$a_1 \in [100, 300], \quad a_2 \in [350, 650], \quad a_3 \in [-10, 10], \quad a_4 \in [-5, 5], \quad a_5 \in [70, 200], \quad a_6 \in [0.01, 0.99].$$

Solving the direct problem, we used two different grids 100×1995 ($\Delta x = 0.03825$, $\Delta t = 0.036$) and 100×3990 ($\Delta x = 0.03825$, $\Delta t = 0.018$). In the case of the real ACO algorithm, we used the following parameters:

$$L = 12, M = 16, I = 55, nT = 4, q = 0.9, \zeta = 1.$$

The real ACO algorithm is probabilistic, so we decide to execute them ten times to check the stability.

Table 1 presents values of reconstructed parameters a_1, a_2, \dots, a_6 in the case of two different grids. In both grids, parameters have similar values except parameter a_1 —the thermal conductivity coefficient. For 100×1995 grid, a_1 is equal to 300 and, for 100×3990 grid, the parameter has value 237.91. The initial condition is approximately equal to 569 K and the order of derivative is equal to 0.20 (100×1995) or 0.21 (100×3990). As we can see in Table 1, if the 100×1995 grid is used, then, for the most of sought after parameters, the standard deviation is less than for the 100×3990 grid. This means that, for the first grid, the obtained results from the ACO algorithm were slightly less dispersed than in the case of the second grid.

Table 1. Results of calculation for grids 100×1995 and 100×3990 (a_i —reconstructed value of parameter, σ_{a_i} —standard deviation ($i = 1, 2, \dots, 6$)).

	100×1995	σ_{a_i}	100×3990	σ_{a_i}
a_1	300.00	69.74	237.91	67.78
a_2	569.73	2.02	566.74	3.80
a_3	1.63	0.40	1.52	2.20
a_4	4.72	0.67	5.00	4.27
a_5	198.02	46.05	178.05	51.73
a_6	0.20	0.05	0.21	0.09
value of the functional	246.98		352.88	

In Figure 1, we can see plots of reconstructed function h for two grids. Both plots are similar. The values of the function for the grid 100×1995 are slightly larger than for the second grid. Table 2 presents errors of reconstruction temperature in measurement points. In both cases, these errors are similar and temperature is reconstructed very well. Average errors are a little bit smaller in the case of 100×3990 grid, but, in the case of maximal errors, it is otherwise.

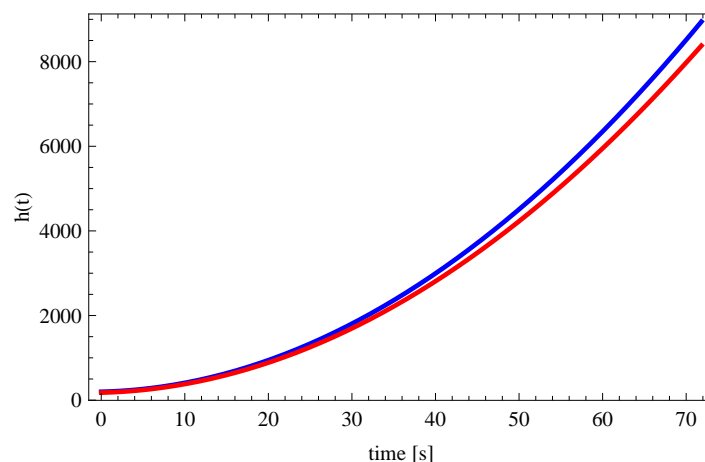


Figure 1. Plots of reconstructed function h for grid 100×1995 (blue line) and grid 100×3990 (red line).

Table 2. Errors of temperature reconstruction in measurement point $x_p = 3.825$ for grids 100×1995 and 100×3990 (Δ_{avg} —average absolute error, Δ_{max} —maximal absolute error, δ_{avg} —average relative error, δ_{max} —maximal relative error).

	100×1995	100×3990
Δ_{avg} [K]	4.92	4.77
Δ_{max} [K]	11.04	12.38
δ_{avg} [%]	1.06	1.02
δ_{max} [%]	3.08	3.46

At the end of this section, we would like to present plots of reconstructed temperature and distribution of errors of this reconstruction (Figures 2 and 3). Temperature reconstruction and distribution of errors are very similar.

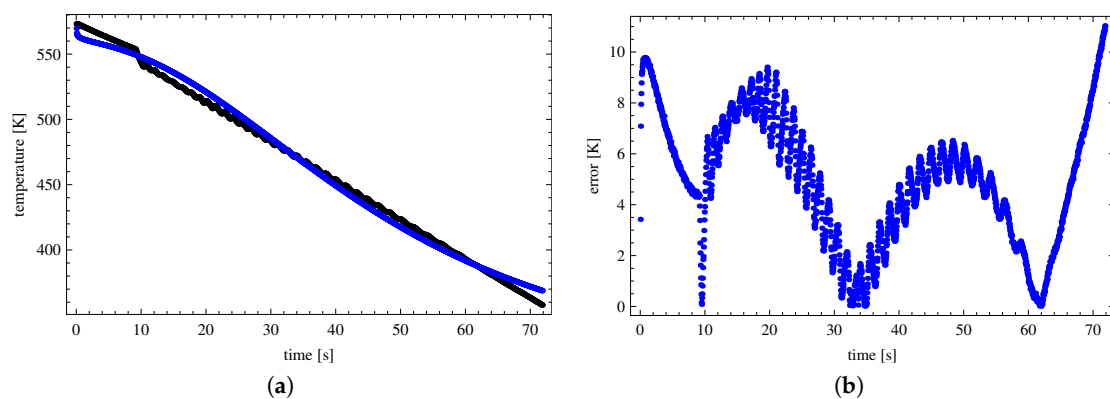


Figure 2. (a) Measurements of the temperature (black line) and reconstructed temperature (blue line); and (b) distribution of errors for this reconstruction (100×1995).

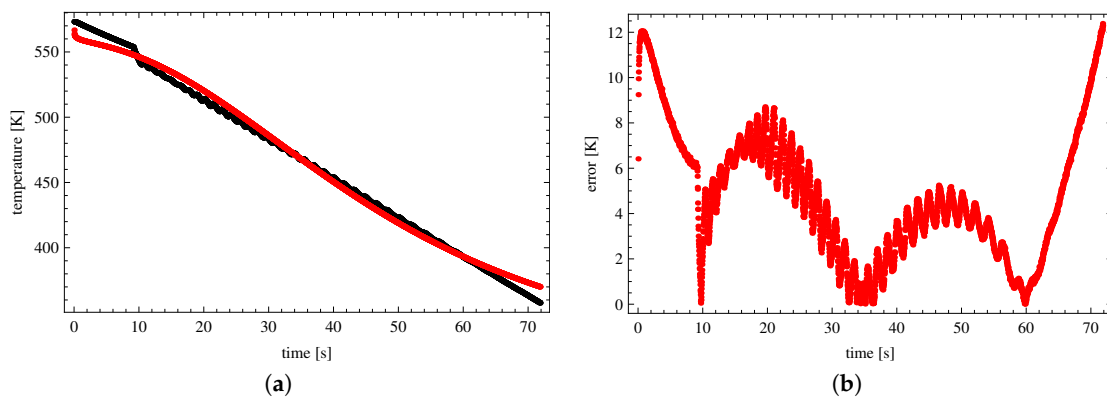


Figure 3. (a) Measurements of the temperature (black line), reconstructed temperature (red line); and (b) distribution of errors for this reconstruction (100×3990).

6. Conclusions

In summary, the paper presents a fractional heat conduction equation with Caputo derivative. Based on this equation, the inverse problem is solved using temperature measurements from porous aluminum. Next, computed values of temperature were compared with real data. First of all, the results obtained were very good. Average relative error of reconstruction was equal to 1.06% for 100×1995 grid, and 1.02% for 100×3990 grid. More density grid gives us smaller relative errors, but a little bit higher maximal errors. Using less density, grid results obtained from the ACO algorithm were less dispersed. The sought order of fractional derivative is approximately 0.20. In the

future, we would like to take under consideration other models of heat conduction using different fractional derivatives.

Acknowledgments: The authors would like to thank the reviewers for their constructive comments and suggestions.

Author Contributions: Mariusz Król, Grzegorz Matula and Waldemar Kwaśny created a sample of porous aluminum, and then made an experiment involving the heating and cooling of the sample. Temperature measurements are the result of experiment; Rafał Brociek and Damian Słota have developed an algorithm for solving direct and inverse problems. They performed a numerical experiment, analyzed the data and wrote the paper.

Conflicts of Interest: The authors declare no conflict of interest.

References

- Podlubny, I. *Fractional Differential Equations*; Academic Press: San Diego, CA, USA, 1999.
- Guo, B.; Pu, X.; Huang, F. *Fractional Partial Differential Equations and Their Numerical Solutions*; World Scientific: Singapore, 2015.
- Ortigueira, M.D. *Fractional Calculus for Scientists and Engineers*; Springer: Berlin, Germany, 2011.
- Das, S. *Functional Fractional Calculus for System Identification and Controls*; Springer: Berlin, Germany, 2008.
- Povstenko, Y.; Klekot, J. The Cauchy problem for the time-fractional advection diffusion equation in a layer. *Tech. Sci.* **2016**, *19*, 231–244.
- Abdeljawad, T. On conformable fractional calculus. *J. Comput. Appl. Math.* **2015**, *279*, 57–66.
- Liu, H.Y.; He, J.H.; Li, Z.B. Fractional calculus for nanoscale flow and heat transfer. *Int. J. Numer. Methods Heat Fluid Flow* **2014**, *24*, 1227–1250.
- Atangana, A. On the new fractional derivative and application to nonlinear Fisher's reaction–diffusion equation. *Appl. Math. Comput.* **2016**, *273*, 948–956.
- Freeborn, T.J.; Maundy, B.; Elwakil, A.S. Fractional-order models of supercapacitors, batteries and fuel cells: A survey. *Mater. Renew. Sustain. Energy* **2015**, *4*, doi:10.1007/s40243-015-0052-y.
- Błasik, M.; Klimek, M. Numerical solution of the one phase 1D fractional Stefan problem using the front fixing method. *Math. Methods Appl. Sci.* **2014**, *38*, 3214–3228.
- Mitkowski, W.; Skruch, P. Fractional-order models of the supercapacitors in the form of RC ladder networks. *J. Pol. Acad. Sci.* **2013**, *61*, 581–587.
- Matušů, R. Application of fractional order calculus to control theory. *Int. J. Math. Models Methods Appl. Sci.* **2011**, *5*, 1162–1169.
- Povstenko, Y.Z. Fractional heat conduction equation and associated thermal stress. *J. Therm. Stresses* **2004**, *28*, 83–102.
- Yang, X.J.; Baleanu, D. Fractal heat conduction problem solved by local fractional variation iteration method. *Therm. Sci.* **2013**, *17*, 625–628.
- Murio, D.A. Time fractional IHCP with Caputo fractional derivatives. *Comput. Math. Appl.* **2008**, *56*, 2371–2381.
- Brociek, R.; Słota, D. Reconstruction of the boundary condition for the heat conduction equation of fractional order. *Therm. Sci.* **2015**, *19*, 35–42.
- Murio, D.A. Implicit finite difference approximation for time fractional diffusion equations. *Comput. Math. Appl.* **2008**, *56*, 1138–1145.
- Liu, J.J.; Yamamoto, M.; Yan, L.L. On the reconstruction of unknown time-dependent boundary sources for time fractional diffusion process by distributing measurement. *Inverse Probl.* **2016**, *32*, doi:10.1088/0266-5611/32/1/015009.
- Zhuang, Q.; Yu, B.; Jiang, X. An inverse problem of parameter estimation for time-fractional heat conduction in a composite medium using carbon–carbon experimental data. *Physica B* **2015**, *456*, 9–15.
- Obrączka, A.; Kowalski, J. Modelowanie rozkładu ciepła w materiałach ceramicznych przy użyciu równań różniczkowych niecałkowitego rzędu. In Proceedings of the Materiały XV Jubileuszowego Sympozjum “Podstawowe Problemy Energoelektroniki, Elektromechaniki i Mechatroniki”, Gliwice, Poland, 11–13 December 2012; Volume 32. (In Polish)
- Brociek, R. Implicite finite difference metod for time fractional diffusion equations with mixed boundary conditions. *Zesz. Naukowe Politech. Śląskiej* **2014**, *4*, 73–87. (In Polish)

22. Brociek, R.; Słota, D. Application of real ant colony optimization algorithm to solve space and time fractional heat conduction inverse problem. *Inf. Technol. Control* **2017**, *46*, 5–16.
23. Socha, K.; Dorigo, M. Ant Colony Optimization in continuous domains. *Eur. J. Oper. Res.* **2008**, *185*, 1155–1173.
24. Hetmaniok, E.; Hristov, J.; Słota, D.; Zielonka, A. Identification of the heat transfer coefficient in the two-dimensional model of binary alloy solidification. *Heat Mass Transf.* **2017**, *53*, 1657–1666.
25. Zielonka, A.; Hetmaniok, E.; Słota, D. Inverse alloy solidification problem including the material shrinkage phenomenon solved by using the bee algorithm. *Int. Commun. Heat Mass Transf.* **2017**, *87*, 295–301.
26. Zhang, B.; Qi, H.; Ren, Y.-T.; Sun, S.-C.; Ruan, L.-M. Application of homogenous continuous Ant Colony Optimization algorithm to inverse problem of one-dimensional coupled radiation and conduction heat transfer. *Int. J. Heat Mass Transf.* **2013**, *66*, 507–516.
27. Grysa, K.; Leśniewska, R. Different finite element approaches for inverse heat conduction problems. *Inverse Probl. Sci. Eng.* **2010**, *18*, 3–17.
28. Hristov, J. An inverse Stefan problem relevant to boilover: Heat balance integral solutions and analysis. *Therm. Sci.* **2007**, *11*, 141–160.



© 2017 by the authors. Licensee MDPI, Basel, Switzerland. This article is an open access article distributed under the terms and conditions of the Creative Commons Attribution (CC BY) license (<http://creativecommons.org/licenses/by/4.0/>).